Passively mode-locked ruby laser: a typical construction and its use in stimulated Raman scattering studies

JEAN LOUIS FERRIER,
Nonlinear Optics Laboratory, University of Angers, 49045 Angers, France.

ALFONS PLANNER
On study leave from Nonlinear Optics Division, Institute of Physics, Adam Mickiewicz University, Grunwaldzka 6, 60–780 Poznań, Poland.

GENEVIÈVE RIVOIRE
Nonlinear Optics Laboratory, University of Angers, 49045 Angres, France

On the basis of our experience the construction and operation of a passively mode-locked ruby laser and its application to the excitation of transient stimulated Raman scattering (TSRS) in liquids are reported. The part devoted to the laser includes: a historical outline, the analysis of spectral and temporal profiles of beam in the active cavity, the conditions under which mode synchronization can be obtained with a saturable, absorber, some details on the construction of: the head, optical cavity, system of ruby pumping together with system of laser pulse triggering, and picosecond pulse selector. The part dealing with TSRS gives the basic properties of the phenomenon and results on its threshold excitation power allowing to draw conclusions as to its self-focusing nature, gain of Raman beams in liquids and the influence of relaxation time of Raman-excited vibration T_2 on the amplification process. The end part of the paper gives the results of self-synchronization of modes in a free-running ruby laser, and the results concerning the dependence of the number of picosecond pulses in the train excited within the saturable absorber thickness.

1. Introduction

Theoretically, all lasers can generate short light pulse. The relaxation oscillations (spikes) in the emission of a He-Ne laser [1] are one of the oldest proof of that. Depending on the modulation conditions of the modes oscillating in an active medium, different forms of the pulsed emission are possible: single pulses produced by Q-switched lasers, pulse trains produced by free-running lasers, mode-locked lasers, and so on.

Generation of picosecond light pulses in a mode-locked laser occurs when a number of longitudinal (axial) modes in the active medium bandwidth with well defined phases and amplitudes are built up and coupled together [2, 3]. The phases of these modes are fixed by a modulator while the amplitudes are stabilized automatically when the laser gain is saturated.

The availability of optical pulses having picosecond duration and peak power excess of 10^9 W have risen considerable interest since 1965. Applications [4] have been developed in fundamental physics – picosecond spectroscopy

of solid state materials, especially semiconductors, studies of molecular dynamics in liquids, transient response of quantum systems, etc., and in technological research – controlled termonuclear plasmas, radars, image processing, etc.

The ruby laser, from the point of view of ultra-short light pulses generation, can be easily mode-locked, and for some applications it is competitive with the most commonly used Nd : YAG or Nd : Glass laser [5]: it can be visually observed and easily photographed. Moreover, it is not affected by the frequency chirp effect: the duration τ of the pulses and their spectral width $\Delta\nu$ verify the theoretical relation $\tau\Delta\nu\sim1$, in contrast to the case of Nd : Glass laser, where $\tau\Delta\nu\sim15$ without corrective devices [6, 7]. In consequence, the stability of duration and spectral width of pulses in the same train are better for the ruby laser. Theoretical values which can be obtained with the ruby are $\tau\sim3\cdot10^{-12}$ s and $\Delta\nu\sim300$ GHz: practically the mode-locked ruby laser is suitable when light pulses of 10 to 1000 ps duration and not too wide linewidths are required.

We show, after a short theoretical analysis and historical review of the development, the ruby laser with passive mode synchronization designed and put in operation by us. The laser was applied to stimulate Raman scattering in our study of transient behaviour of the process.

2. Theory

2.1. Spectral and temporal profiles in the laser cavity

Spectral profile $\Gamma(\omega)$ of the laser cavity is a product of two profiles: the fluorescence line $G(\omega)$ of the active material and the resonance line of the cavity $\gamma(\omega)$ — the modes profile (see fig. 1) [8, 9]:

$$\Gamma(\omega) = G(\omega)\gamma(\omega) = \left[\sum_n \delta(\omega-\omega_n)\exp(j\Psi_n)\right] \times G(\omega)\otimes(\omega), \qquad (1)$$

with

$$\gamma(\omega) = \sum_n g(\omega-\omega_n)\exp(j\Psi_n)$$

and

$$g(\omega-\omega_n) = \delta(\omega-\omega_n)\otimes g(\omega).$$

Temporal profile $\Phi(t)$ is a Fourier transform of $\Gamma(\omega)$, thus

$$\Phi(t) = f(t)\left[\sum_n G(\omega_n\exp(j\omega_n t+j\Psi_n),\right] \qquad (2)$$

where $f(t)$ is a Fourier transform of $g(\omega)$, $\omega_n = \omega_0+n\pi c/L$, n — number of successive modes starting from the top of the fluorescence line, c — light velocity, L — distance between laser mirrors, Ψ_n — phase of the mode n, $\delta(\omega-\omega_n)$ —

Dirac delta, and the following relation is fulfilled

$$\int\limits_{-\infty}^{+\infty} G(\omega)\exp(j\omega t)\,\delta(\omega-\omega_n)\,d\omega = G(\omega_n)\exp(j\omega_n t).$$
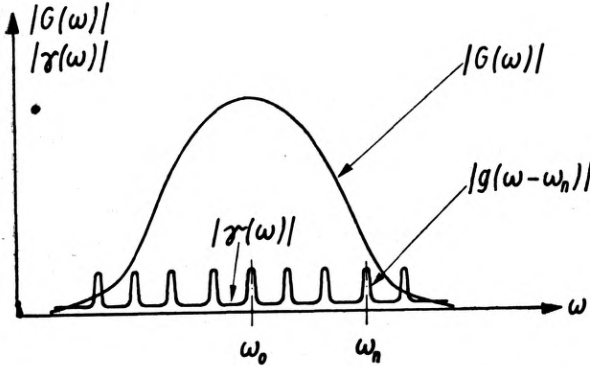

Fig. 1. Spectral profile of the fluorescence line $G(\omega)$ of the active material and of the resonance line of the laser cavity $\gamma(\omega)$

For a free-running laser the phases Ψ_n fluctuate randomly, and $\Phi(t)$ has the characteristics of a thermal noise [10]. In this case the average power of a laser beam is proportional to the number of the excited modes as the following relation holds:

$$\langle|\Phi(t)|^2\rangle_t = |f(t)|^2 N G_0^2. \tag{3}$$

For the ideal case of a mode-locking, Ψ_n is constant, and if $\Psi_n = 0$, the eq. (1) becomes

$$\Phi(t) = f(t)\left[\sum_n \delta(t-2nL/c)\otimes F(t)\right] = f(t)\,x\left[\sum_n F(t-2nL/c)\right], \tag{4}$$

where $F(t)$ is a Fourier transform of $G(\omega)$.

The mode-locked laser emits a pulse train:
— in which the pulses appear at the points $t = 0,\ \pm 2L/c,\ \dots,\ 2nL/c$, and the distance between any two pulses is $T = 2L/c$;
— the envelope of the pulses is determined by $F(t-2nL/c)$, and thus by $G(\omega)$, if the fluorescence line $G(\omega)$ is large the pulses are short;
— the duration τ of each pulse depends of $F(t)$, i.e. $G(\omega) - \tau$ is inversely proportional to the linewidth $\Delta\nu$ of the fluorescence:
— the average power of the laser beam is proportional to N^2, since:

$$\langle|\Phi(t)|^2\rangle_t = |f(t)|^2 N^2 G_0^2. \tag{5}$$

The mode-locking can be active [11, 12] or passive [13–17]. An auto mode-locking can also be obtained (see Appendix A). The passive mode-locking is mostly used and will be briefly studied now.

2.2. Passive mode-locking

A saturable absorber [18, 19] is used to lock in phase the modes in the cavity. The construction of the picosecond pulses allowed by this absorber can be

described schematically as follows [20, 21]:

— At the beginning of the pumping, the atoms in the active material have a random spontaneous emission leading to pulses of various intensities and duration.

— While approaching the treshold the initial noise reflected by the mirrors is amplified. When it becomes far larger than the spontaneous emission, the field is periodically correlated at times t and $t+T$.

— The threshold is more quickly obtained for the modes positioned near the center of the fluorescence line $G(\omega)$: these modes are amplified preferentially. At this level, the laser is still a linear amplifier, and the wave is quasi-periodic (period T).

— However, the linearity of the saturable absorber begins to appear as the intensity increases. The transmission is better for the most intense pulses, and the duration of the pulses is reduced at each passage in the saturable absorber, because the absorption is higher for their rise-front. The energy concentrates in one (or several) high pulses in each period T.

— Thereupon the saturable absorber is completely transparent for a short time and then a strong amplification of the pulse takes place in the active medium.

— After each transition of the saturable absorber the pulse is strongly amplified so that finally a train of pulses with the following period $T = 2L/c$ is obtained at the output of the resonator.

It is important to notice that this description of the train pulses construction is qualitative; a regular train of single ultra short pulses can be produced only at a certain probability. The time distribution of the radiation is not always reproduced from one flash to another [13].

2.3. Some considerations on the saturable absorber

The saturable absorber (and its solvent) must have an absorption line at the frequency of the laser line, a linewidth equal to or larger than that of the active material, a short relaxation time (shorter than T) to play a role for each pulse, and a good stability in the time and with temperature [18, 22].

For the ruby laser, D.D.I. (1,1′ diethyl - 2,2′ dicarbocyanine iodide) in methanol is the most commonly used absorber (absorption peak 706.0 nm, absorption linewidth 30.0 nm, relaxation time 14 ps).

The saturable absorber cell must be in contact with one of the mirrors in the laser cavity, to avoid the generation of two pulses at each back and forth pass in the cavity [23–25]. The duration of the pulses decreases with the length of the cell [26] – shorter pulses (2.5 to 8 ps) were obtained with a 30 μm cell.

2.4. Conclusions for the construction and performances of a mode-locked ruby laser

The pumping near the threshold is necessary to obtain a single pulse during the period T: the time during which the saturable absorber is active is shorter and

less efficient when the gain in the amplifying medium is higher. If several pulses in the period T are present at the end of the linear amplification phase, in the laser beam several pulses can be obtained. A single pulse in time T is easier to obtain when the laser works near its threshold.

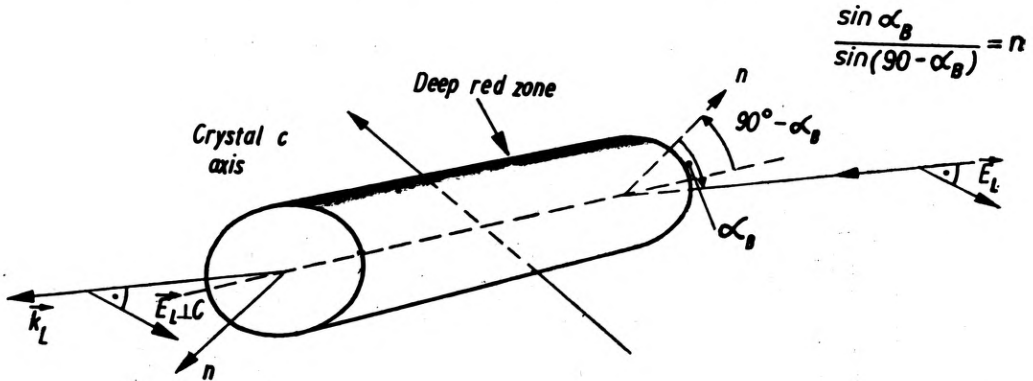A ruby rod with surfaces cut off at Brewster angle (see fig. 2), and anti-

Fig. 2. Orientation of the and surfaces (inclined at the Brewster angle a_B to the laser beam) of the ruby rod with respect to the plane c, and the cylinder axis. The plane c traverses the cylinder and the crystal axis c (deep red zone) which can be seen when the ruby crystal is viewed laterally. The E vector of the laser radiation is perpendicular to the plane c. The best-quality ruby is grown with axis c at 60° to the boule axis [33]

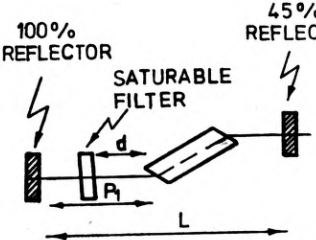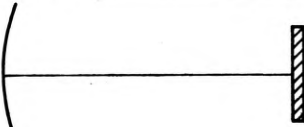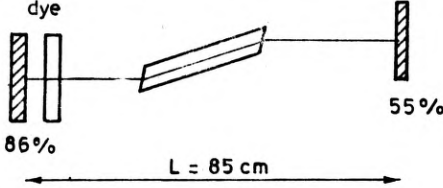reflective coatings prevent the formation of parasitic Fabry-Pérot selectors in the cavity.

The power densities obtained with the mode-locked lasers – 10^9 W/cm² – reach the breakdown limit of the commercially available optical components. Therefore, when choosing the components this problem should be taken into account and to avoid burns both the saturable absorber and the optical devices should be well cleaned, each time the laser is planned to work. To protect the laser from damage and make the stimulation of higher transverse modes more difficult, a diaphragm limiting the power density of the light flux (maximally ca. proportional to the squared pinhole diameter) is also placed in the oscillator cavity [27].

In conclusion, for a given ruby rod, we must adjust the concentration of the saturable absorber, the pumping energy and the reflection coefficients of the mirrors in order to obtain the convenient pulse number and energy output.
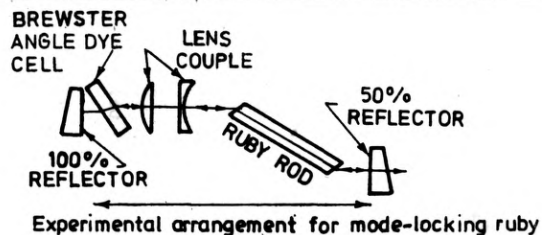
3. Historical review

The first coherent light emission from a ruby laser was obtained in 1960 [28], and the first picosecond pulse trains were produced in mode-locked ruby laser in 1965, with an active mode-locking [29], and a little later with a passive

Table 1. A brief historical review of the passively mode-locked ruby laser

| Reference	Laser diagram	Performance and observations
1	2	3
H. W. MOCKER and R. J. COLLINS [30] 1965	100% REFLECTOR — SATURABLE FILTER — 45% REFLECTOR — for the best results: L = 92.9 cm, d = 4.8 cm, l = 52.8 cm, l = 13.2 cm	With a filter composed of cryptocianine in methanol (absorption 24%), mode-locking is better when the distance d is larger. Estimated pulse duration is 1 ns.
C. M. STICKLEY [33] 1966	98% Curvature radius 4.21	With the plano-convex cavity: — divergence is 4 times smaller than in plano-plano cavity, — a brightness gain of 100 is observed, — a very good stability of the pulse train is obtained (pulse duration not indicated).
V. I. MALYSHEV, A. S. MARKIN, A. A. SYCHEV [34] 1967	dye — 86% — 55% — L = 85 cm — A diaphragm (diameter 4 mm) is put inside the cavity (without any precision on its position)	With a saturable absorber composed of cryptocyanine in nitrobenzol (absorption 38%), a train of 10 pulses is obtained. The duration of each pulse (800 ps) seems to be due to the measurement device. (Remember that considerable difficulties were enocuntered in the first measurements of short times because of some erroneous methods [13]). The linewidth is 3 cm^{-1}.

M. E. Mack [5]
1968

BREWSTER ANGLE DYE CELL
LENS COUPLE
50% REFLECTOR
RUBY ROD
100% REFLECTOR

Experimental arrangement for mode-locking ruby

L_1 — plano-concave, f = 50 mm,
L_2 — plano-convet, f = 100 mm,
55 cm < L < 230 cm

L_1 and L_2 reduce the divergence of the laser beam ($< 10^{-3}$ rad). The reflection coefficient of the output mirror is not critical ($35\%/_0 < R < 70\%/_0$). The choice of the saturable absorber and of its solvent is critical. The best seems to be DDI in methanol. Pulse duration of 2 to 4 ps are obtained (see previous comment about short times measurement), with a linewidth of 6 cm^{-1}. A severe mirror damage problem is noticed.

R. Cubeddu,
R. Polloni,
C. A. Sacchi and
O. Svelto [35]
1969

Saturable Absorber
90°-∝
A Output beam
C
B
90°-∝
Ruby Rod
Output beam

Rooftop prism cavity
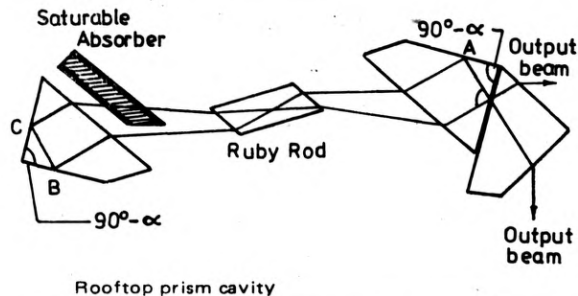
Highly reproducible pulses of 5 ps (see previous comment) are due to the addition of rhodamine 6G to the solution of DDI in methanol. Roof top prisms prevent damages on the mirrors and allow single transverse mode operation.

S. Saikan and
H. Takuma [36]
1971

Ø 6,5 mm
180 mm
50%
T
D 100%

T — inverted telescope,
D — antireflective dye cell
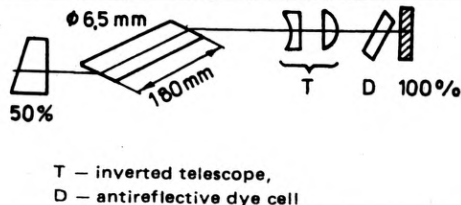
The laser produces pulses of 20 to 40 ps, with a power 0.8 to 2 GW.

H. Jelinkova,
K. Novotny,
M. Vrbova,
K. Hamal [22]
1975

A new passive mode-locker is used: a modified DDI, with a spectral absorption peak at 694 nm instead of 707 nm, a low saturable intensity, and a good temperature and long terme stability. It leads to a best output energy and a faster switching for a given pumping level. It is unfortunate that modified DDI dye is not available, in Jelinkova's labs either.

mode-locking [30]. Later, only passive mode-locking seemed to have been developed. Table 1 presents a historical review of the mode-locked ruby laser, the new principal features and performances being marked at each step.

Mode-locked ruby lasers constructed actually take into account these ameliorations proposed since 1965. Most parts are built in reserach laboratories because only a few constructors [31, 32] agree to make these systems. The next part of this work presents a description of a mode-locked ruby laser built in our laboratory.

4. Construction of a mode-locked ruby laser

The construction of a single stage ruby laser (oscillator), phase mode-locked by a saturable absorber the thickness of which can be varied, is presented. A single pulse can be selected by a fast optical shutter.

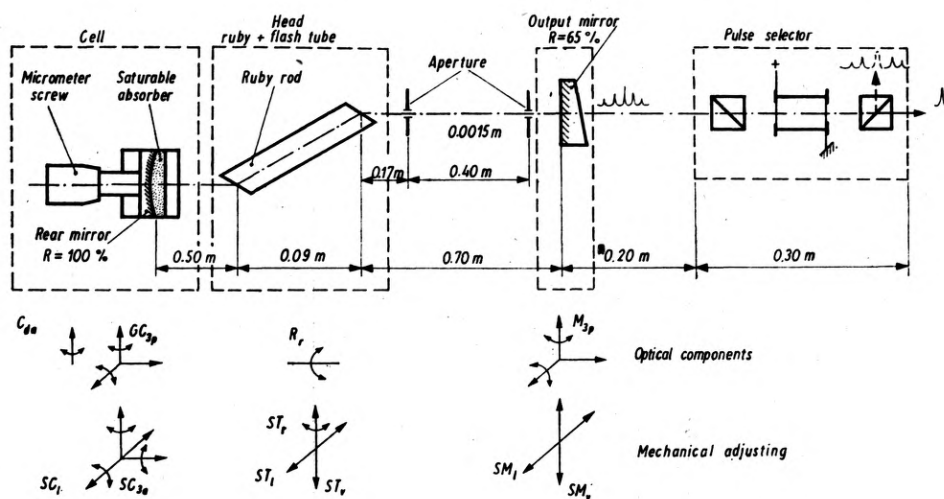The arrangement of optical and mechanical elements in the laser is shown

Fig. 3. Arrangement of optical elements in the constructed passively mode-locked ruby laser. To obtain a single pulse from the picosecond pulse train, the laser oscillator is followed by a pulse selector with a fast optical gate (rise-time $\sim 10^{-9}$ seconds). By replacing the ruby rod, saturable dye and mirrors, the laser can be operated with Nd: YAG, Nd: Glass or other rods:

C — cell, SC — cell support, GC — cell plate, ST — head support, R — ruby, SM — mirror support, M — mirror, l — lateral, da — angular adjustment, v — vertical, r — rotation, $3a$ — 3 axes, $3p$ — 3 points

in figs. 3 and 4, while its operation characteristics are summarized in table 2. Oscillogram of the pulse train emitted by the laser is shown in fig. 5.

As an important results, we observe a good stability of the energy of the pulses (train or single pulse) The alignement of the laser assures its good stability lasting for weeks.
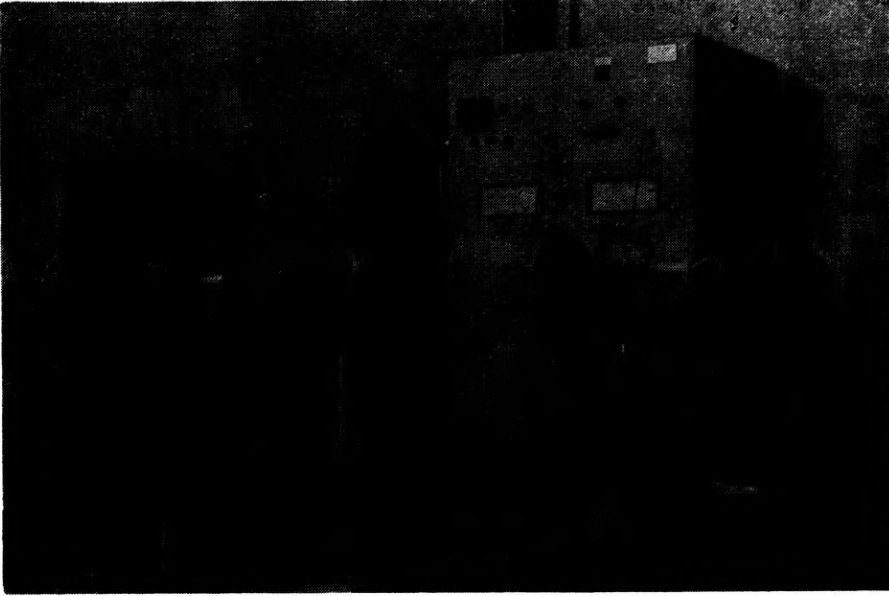
Fig. 4. Photograph of the passively mode-locked ruby laser on the marble bench. When viewing from the left it may be seen the picosecond pulse selector, output mirror, black diaphragm, laser head, and container with dye and movable mirror. Behind the bench, the power supply
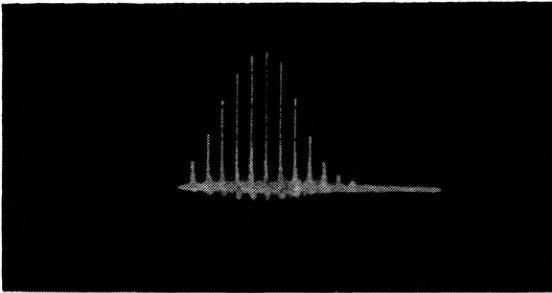

Fig. 5. A train of repetitive light pulses excited in the laser setup shown in fig. 4. For detection of the light a fast photoelectric cell type TF 50 M1 (ITL – rise-time 100 ps) connected to the oscilloscope 7104 (Tektronix – rise-time ~400 ps) was applied. Sweep speed 20 ns/division

When the thickness (*e*) the saturable absorber cell is varied without changing the concentration of the absorber, the number N of the pulses in the train changes. We have measured the pulse number N as a function of *e*. The results are shown and explained in Appendix B. We present in the following part the details of the construction.

4.1. The laser oscillator

A marble supports three parts of the oscillator: the head (ruby with its pumping and cooling accessories), the saturable absorber cell with the totally reflective cavity mirror, and the output mirror. Table 3 gives the principal charac-

Table 2. Performance of the mode-locked ruby laser; shown in fig. 4

Pulse number in a train	20
($Tg = 60\%$ for a saturable absorber thickness (1 mm)	
Time separation between the pulses in the train	8 ns
Polarization of the pulse train	horizontal
Polarization of the single pulse	vertical
Transverse structure	monomode TEM$_{00}$
Beam diameter (2 m after the output mirror)	2 to 2.5 mm
Pulse duration	70 ps
Pulse train energy	30 mJ
Train stability S_{10}–S_{20} *	52–75
Single pulse energy	1 mJ
Single pulse stability S_{10}–S_{20}	55–83
Mean power of one pulse in the train	21 MW
Selected single pulse mean power	14 MW
Mean power density of one pulse in the train	0.6 to 0.7 GW/cm²
Mean power density of the selected single pulse	0.45 GW/cm²

* S_{10} is the rate of the shots having an energy equal to the mean energy $E_m \pm 10\%$, S_{20} has the same definition with $E_m \pm 20\%$.

Table 3. Principal characteristics of the optical and mechanical components of the laser in fig. 4

Component	Characteristics	Observations
Ruby rod	Diameter $\varnothing = 6.35$ mm length $l = 100$ mm Brewster (Brewster's angle at the ends) quality: Schlieren	A mechanical device (pinio + rack) allows the rotation of the ruby around its axis, in order to put its faces vertically
Xe flash tube	Type FX-81C-4 EG&G mini voltage: 1 kV mini triggering voltage: 25 kV	The insulator used for the high voltage arrivals is "vitreous ceramic" Macor-Corning Glass
Head cavity	Pseudo-elliptical (dimensions on fig. 7), made in brass with a chromium deposite	A water-cooling is necessary
Totally reflective mirror	SiO$_2$ with coating for 694.3 nm plano-concave $R = 2.4$ m diameter: 25 mm thickness: 9.5 mm	The mirror can be displaced by a micrometer screw in order to vary the thickness of the absorber cell (fig. 3)
Saturable absorber cell	Absorber is D.D.I. in methanol the thickness e of the cell can be varied between 0 to 2 cm, a mini pump ensures the circulation of the liquid after each shot	The impermeability of the cell is allowed by a Viton joint
Output mirror	SiO$_2$, with coating, $R = 65\%$ at 694.3 nm plane-plane (prismatic $\alpha = 30'$) diameter; 25 mm, thickness: 9.5 mm, second face antireflected	

teristics of the optical components and the way of adjusting the mechanical systems in the laser oscillator. The construction of a single lamp head is shown in figs. 6 and 7.
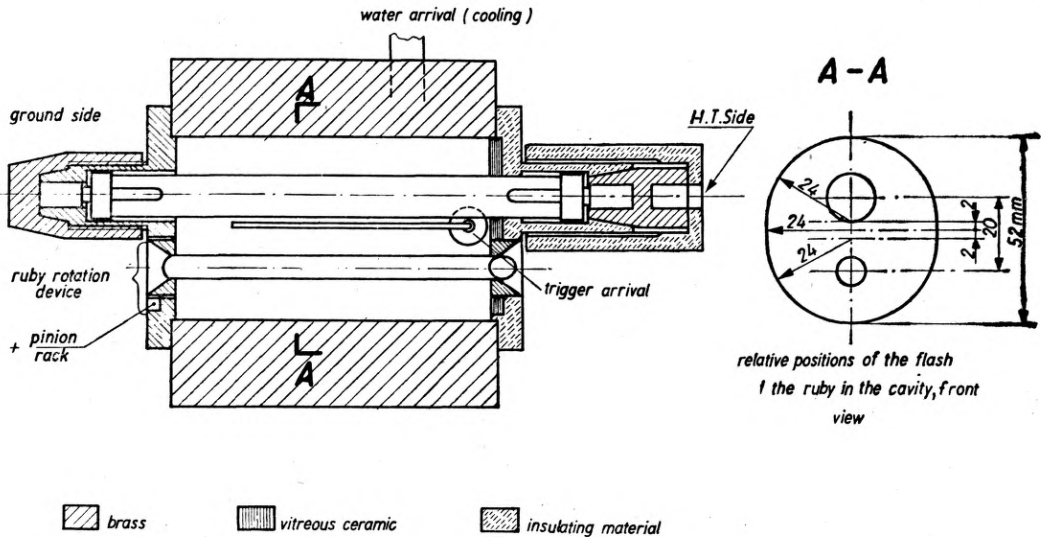

Fig. 6. Section view of the ruby laser head

4.2. Electronic part of the laser

The electronic part of the laser includes:
— power supply with high voltage stabilization,
— flash tube ionizer,
— laser flash programmer,
— picosecond pulse selector.
The functioning of the aforementioned sets is described below.

4.2.1. Power supply with high voltage stabilization

A block diagram of the power supply for capacitor discharge bank is presented in fig. 8. The power supply operation is based on the classical principle: the thyristor control unit influences the effective value of voltage supplying the primary winding of H.V. transformer, while its secondary winding loads the capacitor discharge bank through a rectifier. The bank's output is connected with an executing unit of an ionizer, i.e. with a Tesla transformer (in former set the flashtube was ionized by applying external high voltage from the ionizer shown in fig. 10b).

Voltage stabilization operation is based on producing the error voltage (proportional to the value of voltage to be stabilized) as the function of the angle of current flowing through the thyristor control unit. The conversion
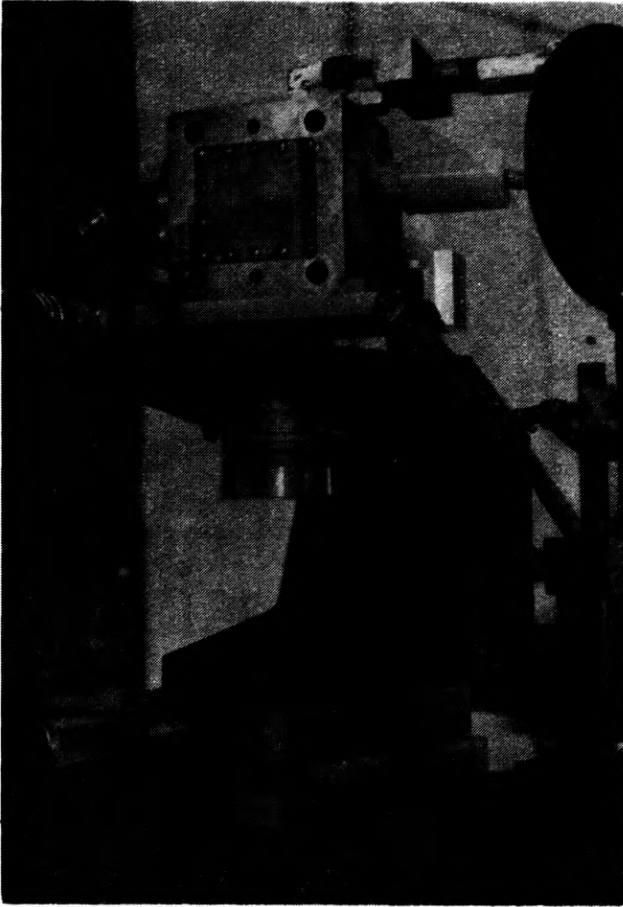
Fig. 7. Photograph of the laser head and its fixing to the marble optical bench
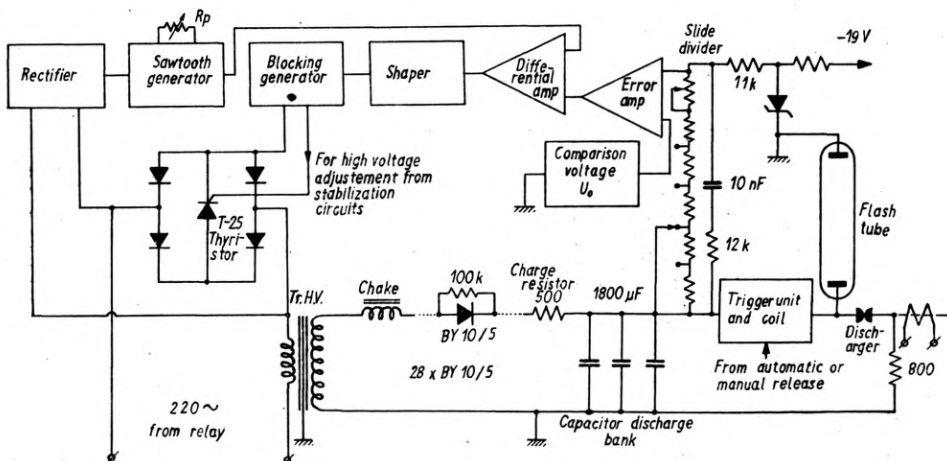

Fig. 8. Block diagram of the power supply with high voltage stabilization, applied to load the discharge battery connected to the flash tube

of amplitude into time is synchronized with the change of voltage in network, and the thyristor control unit is released by pulse. The scheme of stabilization system is shown in fig. 9. Both comparison voltage signal U_0 and stabilization
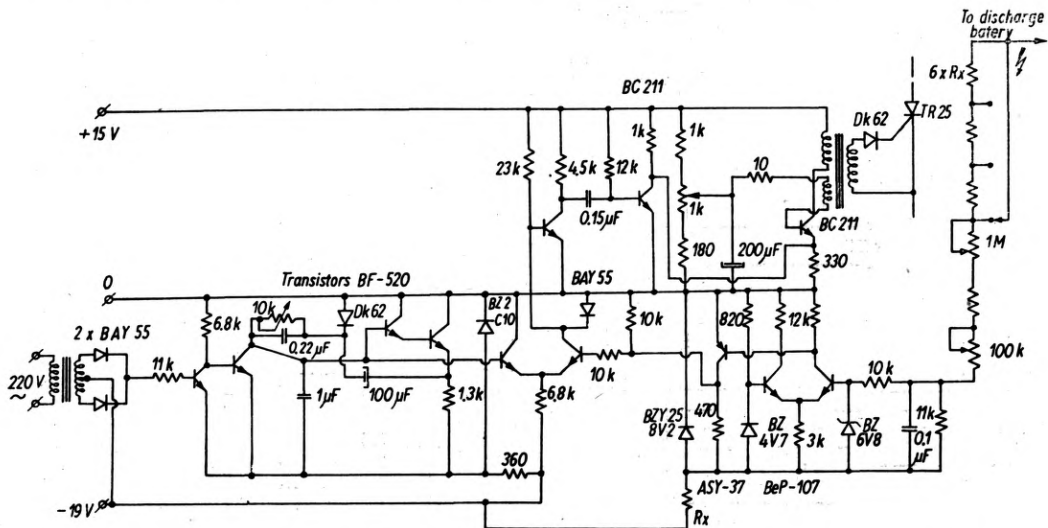

Fig. 9. Diagram of the electronic circuit for stabilization of the high-voltage supply, shown in fig. 8

voltage from a resistance divider are applied simultaneously to an error amplifier. A differential voltage appearing at the output of the amplifier is next applied to a differential amplifier, at the output of which a voltage appears (at the moment when the instantaneous value of sawtooth voltage is equal to the error voltage). The feedback in transistor emitters of differential amplifier is so high that when the sawtooth voltage is lower than the error voltage, the voltage at the amplifier output disappears. If the instantaneous value of the sawtooth voltage becomes equal to the error voltage, the aforementioned feedback causes a jump in voltage which is next differentiated in the differentiating system. The pulses obtained release a monostable self-chocking generator (blocking generator) to control the power of the thyristor gate with a pulse. Due to the error voltage the pulses releasing the thyristor are moved within the angles 0 and 2π. The dependence between the angle of shift and the error voltage is found to be linear. The stabilization rate depends on the line slope angle, which, in turn, depends only on the angle of slope of the linear part of the sawtooth voltage. The change in the line slope is done by selecting the amplitude of the sawtooth voltage with a control of R_p.

4.2.2. Flash tube ionizer

To initiate a discharge in a flash tube two systems of ionization were used: an old car ignition coil [37] – its diagram is presented in fig. 10b; and Tesla transformer, the secondary winding of which is a coil connecting the discharge battery with the flash tube – its diagram is given in fig. 10a. The inductance

of the secondary winding was about 150 µH, and was adjusted to the parameters of the flash tube circuit [38].
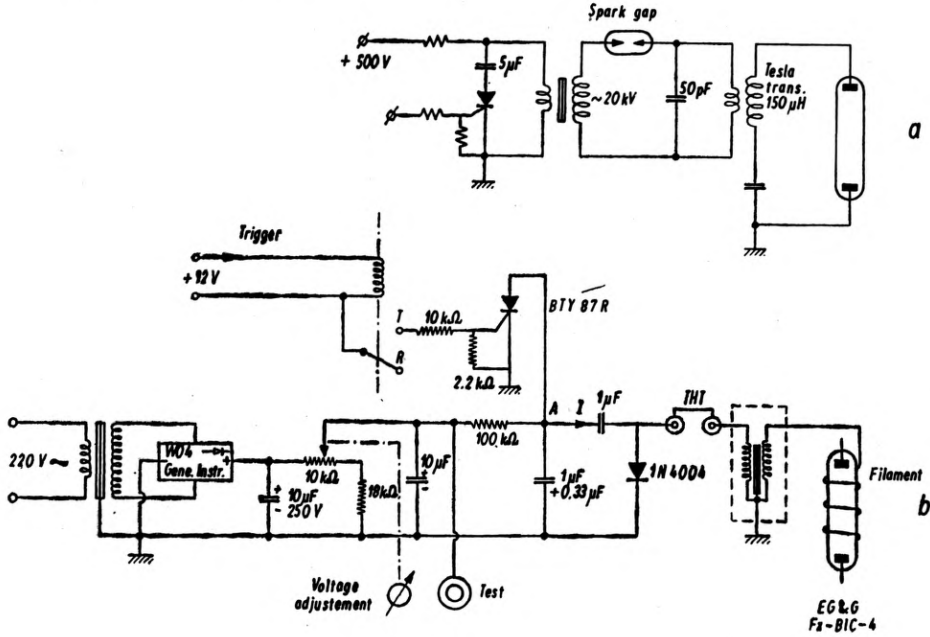

Fig. 10. Diagram of the electronic circuits used to ionize the flash tube:
a — the ionizing pulse (from secondary winding of the Tesla transformer, $L = 150$ µH) is applied directly to the positive electrode of the flash tube; b — the ionizing pulse (from the secondary winding of a car coil) is applied to the wall of the flash tube

4.2.3. Laser shots programming

Programming system produces the electric pulses which release the ionizer and counts the laser pulses. Its main subset is a programmable clock synchronized by network voltage with the frequency of 50 Hz (20 ms). The principle of the programmable clock is shown in fig. 11. The counter of laser pulses indi-
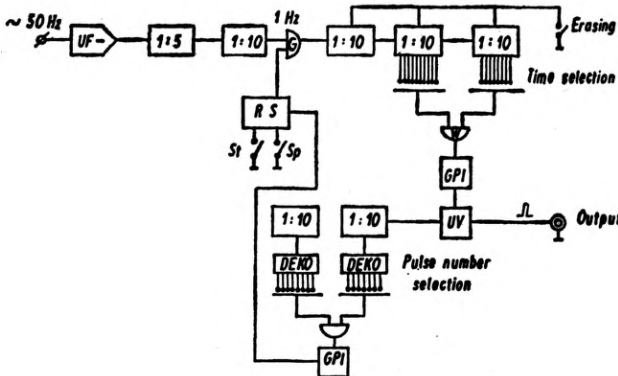

Fig. 11. Block diagram of the circuit for counting and releasing of the laser shots

cates the number of battery discharges, it, however, is not sensitive to flash tube ionization acts.

4.2.4. Picosecond pulse selector

The picosecond pulse selector (general view see fig. 12) is made of Pockels cell between two crossed Glan prisms. Its optical setup is shown in fig. 13. Table 4
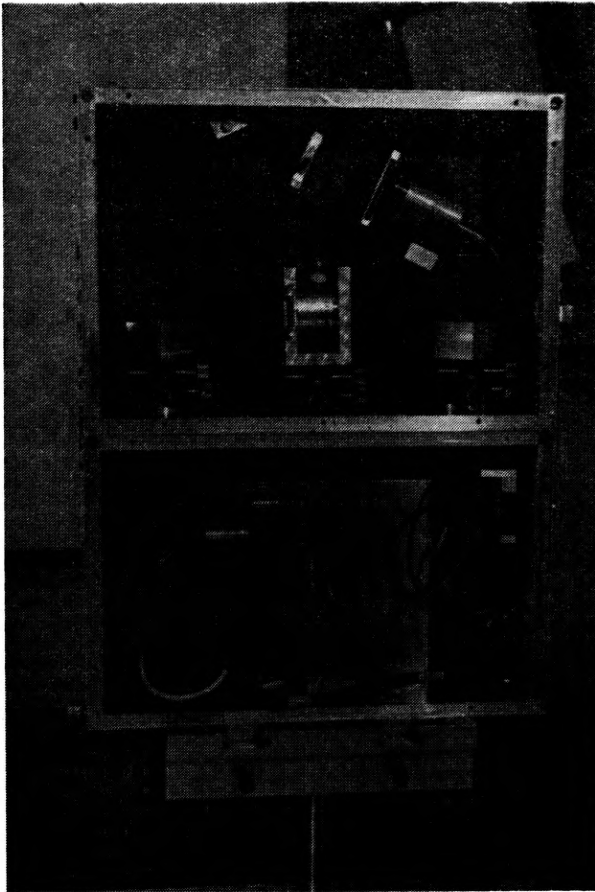

Fig. 12. Photograph of the picosecond pulse selector

Table 4. Characteristics and operation mode of the applied Pockels cell

Pockels cell (Ref. 1057 Lasermetrics)	KDP aperture: 10 mm, max. density power: 750 MW/cm², extinction ratio: 600 : 1, rise-time < 1 ns, $U_{\lambda/2}$ for 694.3 nm: 3950 V	High voltage is applied to the cell during a short time, when the photoelectric cell O_2 (fig. 6) delivers a signal sufficiently high to the ultra fast shutter switch (fig. 7)

gives the characteristics and operation mode of the Pockels cell. The electronic circuits and the chronogram of the pulse selector operation are given in figs. 14 and 15. As the high voltage ultra fast shutter a krytron is used, i.e. a four
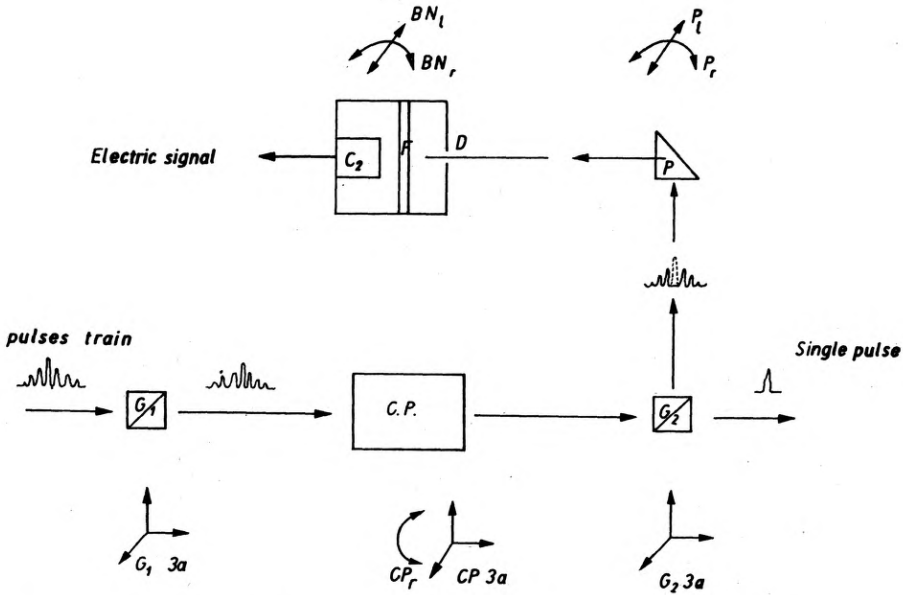
Fig. 13. Arrangement of optical elements in the picosecond pulse selector

$G1$ — glan prism, polarizer; $G2$ — glan prism, analyzer; CP — Pockels cell; P — prism; r — rotation; l — lateral; $3a$ — 3 axes;

$B.\ N.$ — "black box" $\begin{cases} D - \text{diaphragm (adjustable)} \\ F - \text{filters} \\ C_2 - \text{photoelectric cell} \end{cases}$

Signal emitted by the photocell C_1 illuminated by the flash tube.

Output signal in point C (fig.14), (if the krytron does not commute between t_o and t_1) adjustable amplitude.

Krytron gate signal, after the laser shot is detected by C_2 (rise-time some ns amplitude ~ 750 V).

Output signal in point C_1 if the krytron has commutated, i.e. if the pulse selection has been done.

Voltage on the coaxial line 1, point A.

Voltage on the coaxial line 2, point B.

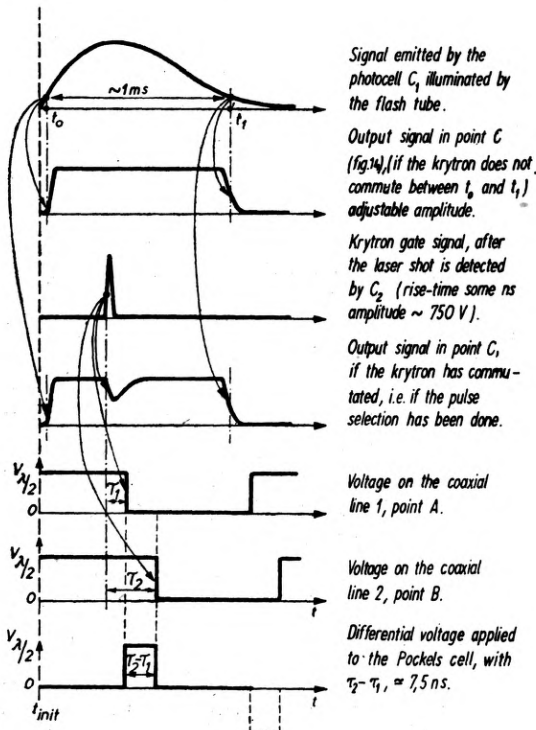Differential voltage applied to the Pockels cell, with $\tau_2 - \tau_1, \simeq 7.5\,ns.$

Fig. 15. Chronogram of the pico-second pulse selctor operation
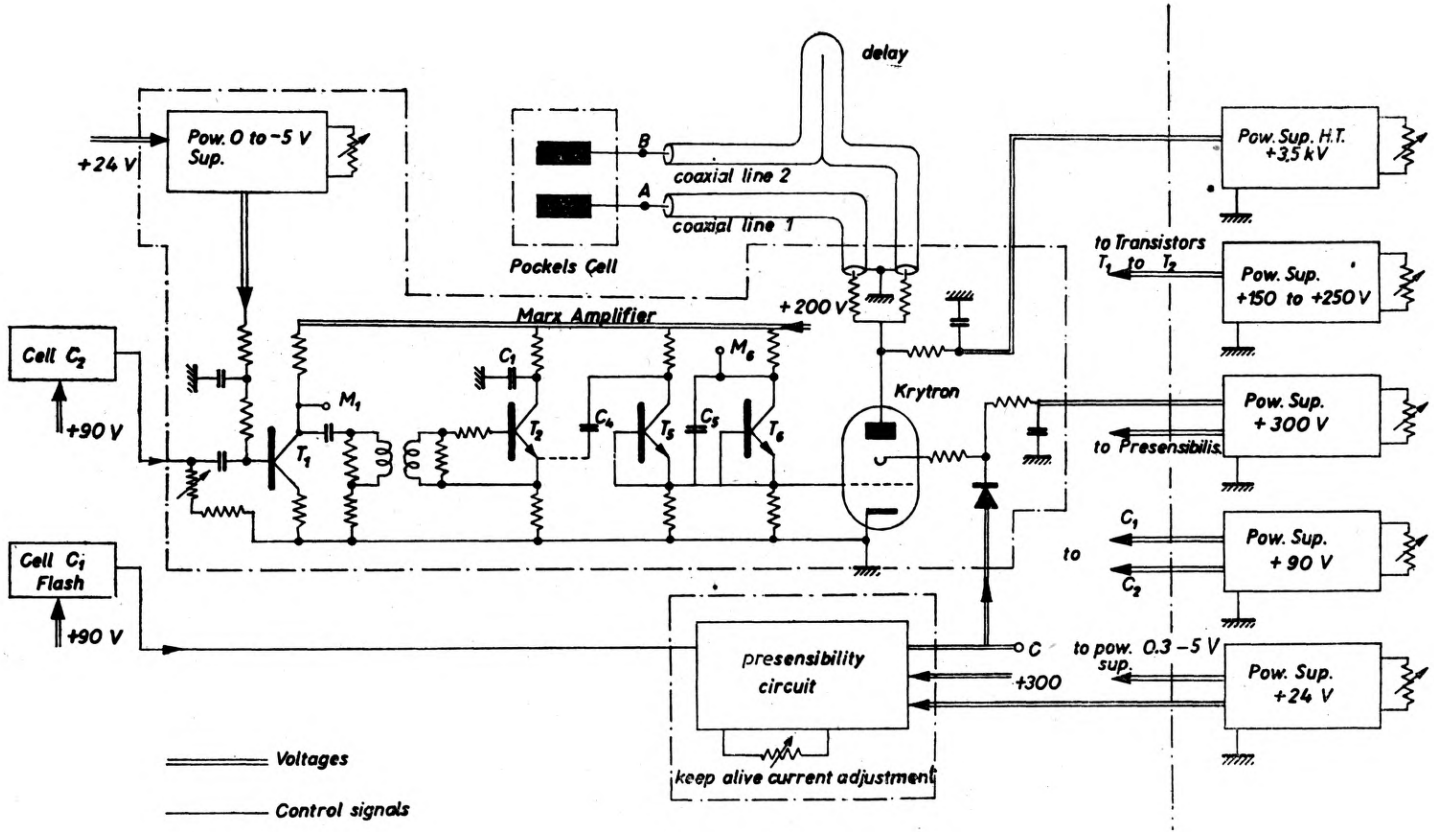
Fig. 14. The electronic circuit of the picosecond pulse selector

-electrode gas tube, activated by a positive voltage at the gate. Its commutation time is small when the voltage applied to the grid is high and of a short rise-time, when a current exists in the keep alive electrode activated by photocell C_1. The Marx amplifier provides such a voltage. The duration of the high voltage pulse in the Pockels cell is determined by the length of the two coaxial lines (1 and 2 in fig. 14). It has to be shorter than the interval between two consecutive pulses in the train (8 ns).

5. Stimulated Raman scattering excited by the mode-locked ruby laser

The operation characteristics and the stability of the laser enable us to use it in various non linear optics experiments, such as wavefront reconstruction or phase conjunction [39, 40], stimulated Raman scattering (SRS) and, particularly, to stude transient stimulated Raman scattering (TSRS).

We present now some results obtained in SRS.

The first experiment in which SRS was excited by subnanosecond ruby laser pulses was carried out by VON DER LINDE et al. in 1969 [41]. The purpose of the authors was to use an excitation short enough to suppress stimulated Brillouin scattering, but long enough to keep a stationary SRS. Moreover, by working far above the SRS threshold, they avoided the effects of self-focusing (SF). So, they were able to compare the theoretical results on stationary SRS with their experimental results, stating a good agreement, which was impossible in earlier works, because of the predominant influence of SF and the Brillouin scattering.

When the exciting pulses have a duration of some picoseconds, SRS can be transient. The nonstationarity condition is [42, 43]:

$$2\tau_p/T_2 \ll G_{SS} = gI_L l, \tag{6}$$

where τ_p is duration of the exciting pulse, T_2 — relaxation time of the Raman excited vibration, I_L — exciting intensity, l — length of the active medium, and g — Raman gain (characteristic of the excited medium).

Theoretical studies [42–44] show that TSRS is characterized by:

— a transient gain, much lower than the stationary gain and independent of T_2,

— a Raman pulse delayed with respect to the exciting pulse, and displaying a shorter duration,

— a large asymmetry in the indicatrix between the forward and backward diffusion.

In experiments conducted with mode-locked ruby laser [45], Carman et al. have verified experimentally some of these properties. By illuminating gaseous SF_6 (pressure $1.82 \cdot 10^6$ Pa) with a pulse train, in which each pulse has a duration of 15 ps, they observed Raman pulses of 9 ps, with a delay of 6 ps, after the exciting pulses, in agreement with the theory.

In several media displaying a low gain in stationary SRS (for instance, water), TSRS has been excited easily; this is explained by the fact that the stationary Raman gain g is inversely proportional to the spontaneous Raman linewidth $\Delta\nu_{sp} \sim 1/T_2$, whereas the transient gain being independent of $\Delta\nu_{sp}$, allows the stimulation of large Raman lines.

SAIKAN [46] verified this property; by comparing for mixed liquids the spectra in nano- and picosecond excitations he observed that the thin lines disappear more quickly in picosecond excitation than the larger ones.

More recently, CHATELET et al. [47] using a train of 15 pulses of the duration of 40 ps and a total power of 50 MW, have excited TSRS in gaseous nitrogen at high pressure. They have stated Raman threshold independent of pressure, i.e of the spontaneous Raman linewidth, contrary to the results obtained in nanosecond excitation. These observations confirm the fact that the transient Raman gain is independent of $T_2 \sim 1/\Delta\nu_{sp}$.

However, in all the experiments, no absolute gain or threshold measurements have been performed and compared with the theory. With the laser described above and a calibrated joulemeter developed in the laboratory [48], we were able to measure the absolute values of the SRS thresholds in various liquids excited by linearly or circularly polarized laser beams [50, 51]. The results are summarized in table 5, where the characteristics of the liquids studied are also given.

Table 5 shows that for a 70 ps exciting pulse duration SRS is, depending on the liquids, in the stationary range (C_6H_{12}) or in the transient range (CS_2) if we use the criteria described in formula (6).

Table 5. Results of threshold study of the first Stokes line of stimulated Raman scattering in the pure liquids. The excitation pulse had a duration of about 70 ps and a wavelength of about $\lambda = 694$ nm, g is the stationary Raman gain, K the self focusing constant, P_{Rm} the measured Raman threshold in linearly polarized light, P_{Rc} the calculated threshold [50] in the same conditions, P_{cir}/P_{Rm} is the measured ratio of the thresholds in circulary and linearly polarized light; all the measurements are made with a 32 cm long cell

Examined liquids	g $\times 10^{11}$ $(W/m)^{-1}$	K $\times 10^{18}$ $(W/m^2)^{-1}$	T_2 ps	$G_{SS}T_2$ ps	P_{Rm} MW/cm^2	P_{Rc} MW/cm^2	P_{cir}/P_{Rm}	Presence of S.F.
CS_2	50	7.6	10.6	5000	200	25	1.8	yes
C_6H_6	3	1	2	220	1100	70	2.1	yes
CH_3COCH_3	1	0.25	0.34	100	6400	200	1.2	doubtly
C_6H_{12}	1	0.07	0.56	45	2500	230	1	no

All the measured thresholds are much higher than the values calculated, when taking account of the transient situation and the self-focusing effects whenever necessary [50, 55]. The observed ratio "measured threshold to calculated threshold" ranged from ~ 10 to 20. These observations confirm those made under different conditions [52], and lead to the same conclusions: the

usual theories do not decribe correctly the transition from the stationary range to the extreme transient one. The phenomena seem to be transient for pulse durations far longer than those predicated by the formula (6). The measurements of the SRS linewidths excited by the same laser lead also to large discrepancies between the calculated and measured values [53]. It seems that the values of g and T_2 deduced from the measurements made in the stationary situation with low exciting powers and introduced into the calculations are inadequate for the picosecond range and the high intensity used.

From the measured values of the ratio P_{cir}/P_{Rm}, we deduce interesting information on the phenomena leading to self-focusing, i.e., on the phenomena described by the constant K. When K is only due to orientational Kerr effect, $(P_{cir}/P_{rect})_{theor} \simeq 4$. The measured values $(P_{cir}/P_{rect}) \simeq 1.8$ or 2.1 indicate a contribution of electronic deformation and of SRS itself in K of the same order as that of molecular orientation [54].

This brief discussion shows that the SRS threshold studies lead to interesting conclusions on the characteristic liquid parameters g and K, especially in the transient range.

6. Conclusion

As a brief conclusion, we note that it is possible to construct a performing and stable mode-locked ruby laser in a laboratory, often using elements which were previously incorporated in free-running or Q-switched ruby lasers (power supplied, mirrors, flash tubes, etc.). The construction of such a laser opens the door to interesting experiments in wide range of fields: the molecular dynamics of liquids, the electronics processes in atoms and molecules, the photo-chemical process, etc. With regard to this we did not hesitate to give an extensive description of the mode-locked ruby laser.

Appendix A

Short pulses obtained with a free-running ruby laser

The ruby laser (see fig. A1) is composed of: a flat mirror with a reflection coefficient $R \cong 100\%$ the laser head, as described in Section 4.1, and a flat mirror with a reflection coefficient $R \cong 65\%$. For most of the geometrical configurations and most values of the flash power supply voltage U, we have noted a light intensity $I(t)$ similar to that usually delivered by free-running lasers.
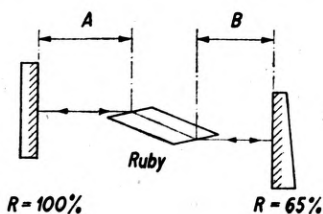

Fig. A1. Setup of optical elements of the resonator of ruby laser with free-emission

However, for some values of A and B, on the one hand, and for some of U values, on the other hand, we do not observe a random signal $I(t)$ but one or two light pulses with a time duration of several hundred nanoseconds (see fig. A2). The delivered signal looks like
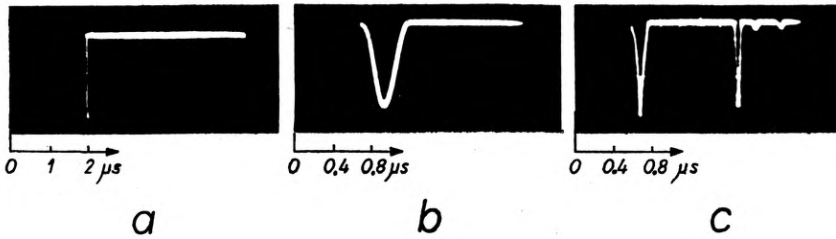

Fig. A2. Oscillograph records of the pulses emitted by the free-running ruby laser shown in fig. A1, in their dependence on the optical resonator parameters: a — $A = 43.0$ cm, $B = 25.5$ cm, $U = 1100$ V, sweep speed: 0.5 μs /division; b — $A = 45.5$ cm, $B = 53$ cm, $U = 1150$ V, sweep speed: 0.2 μs/division; c — $A = 45.5$ cm, $B = 53$ cm, $U = 1300$ V, sweep speed: 0.2 μs/division

that of a Q-swithed laser and can be explained by a kind of "self-locking" of the modes in the cavity because of the nonlinear behaviour of the ruby itself; besides the phenomenon is favoured by an increase of the flash power supply voltage.

Nevertheless, it seems to be difficult to reproduce this phenomenon with good reliability.

Appendix B

Saturable absorber thickness and pulses number for the mode–locked ruby laser

By means of the micrometer screw we can modify the saturable absorber thickness, i.e., its global transmission rate Tg, and by using a fast photoelectric cell type TF 50 M1 (ITL – rise-time 100 ps) connected to an oscilloscop 7904 Tektronix (rise-time 1.8 ns) we can display the pulse train at the laser output and take a photo of it. In our experiments we have worked with a constant pumping voltage (or energy) whatever the saturable absorber thickness was the voltage chosen is by 100 V higher than the laser threshold voltage. The interpretation of the various results is found in table A1, where for a 1 mm saturable absorber

Table A1. The number of repetitive light pulses in the train vs the thickness of the saturable absorber or its global transmission rate Tg

Saturable absorber thickness, mm	0.3	0.5	0.6	0.7	0.8	0.9	1	1.2	1.4	1.6	1.8	.2
Pulses number	36	33	30	25	23	22	21	20	15	13	11	10
$Tg\%$	86	77	73	70	66	63	60	54	49	44	39	36

thickness $Tg = 60\%$, therefore $Tg\% = 100\exp(-0.51\ e)$, e — saturable absorber thickness expressed in mm. If we represent the number of pulses in the train vs. the global transmission rate Tg of the saturable absorber or of its thickness we obtain a relatively straight line (see fig. A3).
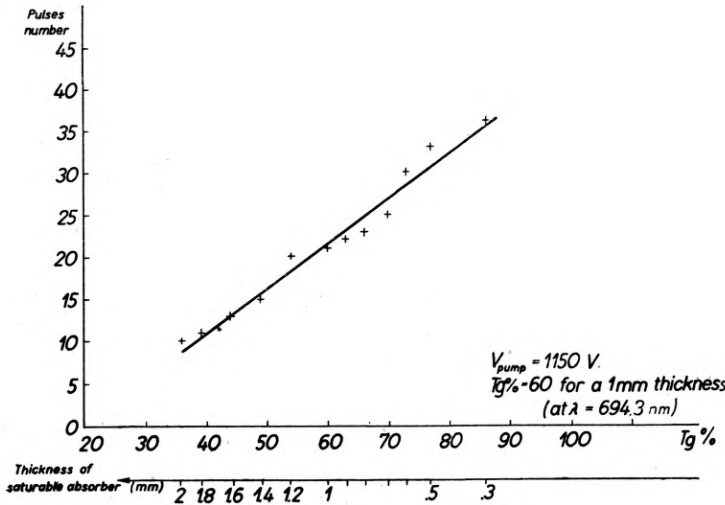

Fig. A3. Number of pulses in the train plotted versus the full transmission Tg of the saturated absorbent and its thickness e

We have noticed that for the equal pumping voltage, the bigger the saturable absorber thickness, i.e., the bigger the losses in the oscillator cavity, the more difficulties for the system to emit a laser beam.

In further experiments we adjust the total transmission rate of the saturable absorber ($Tg = 60\%$, thickness 1 mm), the pumping energy, and the output mirror reflection coefficient in order to get a good selection and temporal compression of a pulse at every back and forth pass of the wave in the cavity, and an energy density inside the cavity under the damage threshold for optical components.

Interpretation of the results

An increase in the losses in the oscillator cavity involves a reduction of its quality factor, the spectral width related to each mode increases, and it provokes a shorter emission duration (let us remenber that the quality factor Q_c of an oscillator cavity is related to the frequency at a resonance ν_R and to its spectral width $\Delta\nu_R$ by $\Delta\nu_R/\nu_R = 1/Q_c$). The time interval between the pulses in the train being set by the cavity geometry ($2L/c$) the number of pulses must diminish with increasing thickness of the saturable absorber, this is precisely what the experiment proves.

We can also affect the losses produced by the saturable absorber by changing its concentration for an identical saturable absorber thickness and an equal pumping voltage.

References

[1] HARGROVE L. E., FORK R. L., POLLACK M. A., Appl. Phys. Lett. **5** (1964), 4.
[2] DE MARIA A. J., Electronics **16** (1968), 112. *Progress in Optics*, Vol. 9, E. Wolf Ed., North-Holland, Amsterdam 1971, 33.

[3] KACZMAREK F., *Introduction to Laser Physics* (in Polish), PWN, Warszawa 1977.

[4] *Laser Handbook*, Vol. 1 and 2, E. T. Arrechi, E. O. Schulz-DuBois Eds.; Vol. 3, M. L. Stitch Ed., North-Holland, Amsterdam 1972.

[5] MACK M. E., IEEE J. Quant. Electron. **QE-4** (1968), 1015.

[6] DE MARIA A. J., STETSER D. A., GLENN W. H., Science **156** (1967), 1557.

[7] TREACY E. B., Phys. Lett. **28A** (1968), 34.

[8] LEFEBRE R., Réalisation d'un Laser à modes bloques on phase, Ph. D. dissertation, Bordeaux I Univ., Talence, France 1975.

[9] FERRIER J. L., Étude et réalisation d'un laser à rubis à modes bloqués en phase, Ph. D. dissertation, Nantes Univ., Angers 1979.

[10] BRADLEY D. J., NEW G. H. C., Proc. IEEE **62** (1974), 313.

[11] HARRIS S. E., Appl. Opt. **5** (1966), 1639.

[12] CROWELL M. H. IEEE J. Quant. Electron. QE-1 (1965), 12.

[13] ZELDOVICH B. YA., KUZNETSOVA T. I. Uspekhi **15** (1972), 25. (transl. from Usp. Fiz. Nauk **106** (1972)), 47.

[14] KRYUKOV P. G., LETOKHOV V. S., IEEE J. Quant. Electron. **QE-8** (1972), 766.

[15] BASOV N. G., KRYUKOV P. G., LETOKHOV V. S., SENATSKII YU. V., IEEE J. Quant. Electron. **QE-4** (1968), 606.

[16] LETOKHOV V. S., JETP **28** (1969), 562 (transl. from ZhETF **55** (1968), 1077).

[17] BASOV N. G. KRYUKOV P. G., LETOKHOV V. S., MATVEETS YU. A., JETP **29** (1969), 830.

[18] PILIPOVICH V. A., KOVALEV A. A., *Opticheskiye kvantovye generatory s prosvetlayush-chimisya filtrami*, ed. Nauka i Tekhnika, Minsk 1975.

[19] GRAJA A., KOWALSKA M., PLANNER A., Fizyka Dielektryków i Radiospektroskopia **4** (1967), 199.

[20] LETOKHOV V. S., MOROZOV V. N., ZhETF **52** (1967), 1296; JETP **25** (1967), 862.

[21] FLECK J. A., J. Appl. Phys. **39** (1968), 3318.

[22] JELINKOVA H., NOVOTNY K., VRBOVA M., HAMAL K., Opt. Quant. Electron **7** (1975), 420.

[23] DE MARIA A. J., STETSER D. A., HEYNAU H., Appl. Phys. Lett. **8** (1966), 174.

[24] GARMIRE E. M., YARIV A., IEEE J. Quant. Electron QE-3 (1967), 222.

[25] WEBER H. P., J. Appl. Phys. **39** (1968), 6041.

[26] BRADLEY D. J., NEW G. H. C., CAUGHEY S. J., Opt. Commun. **2** (1970), 41.

[27] DASZKIEWICZ S., PLANNER A., STEFANIAK T., *Abstracts of the IX Conf. on Quant. Electr. and Nonlinear Optics*, Poznań, Poland, April 23–26, 1980, Section A, 133.

[28] MAIMAN T. H., Nature **187** (1960), 493.

[29] DEUTSCH T., Appl. Phys. Lett. **7** (1965), 80.

[30] MOCKER H. W., COLLINS R. J., Appl. Phys. Lett. **7** (1965), 270.

[31] *Ultrashort Light Pulses*, S. L. Shapiro Ed., Springer-Verlag, Berlin-Heidelberg-New York 1977.

[32] KOECHNER W. *Solid-State Laser Engineering*, Springer-Verlag, New York-Heidelberg-Berlin 1976.

[33] STICKLEY C. M. IEEE J. Quant. Electron. **QE-2** (1966).

[34] MALYSHEV V. I. MARKIN A. S., SYCHEV A. A., Pisma ZhETF **6** (1967), 503.

[35] CUBEDDU R. POLLONI R. SACCHI C. A., SVELTO O., IEEE J. Quant. Electron. **QE-5** (1969), 470.

[36] SAIKAN S., TAKUMA H., Jap. J. Appl. Phys. **10** (1971), 1244.

[37] FERRIER J. L., HANSEN C., Le Haut-Parleur, No. 1652 (1980), 297.

[38] MARKIEWICZ J. P., EMMETT J. L., IEEE J. Quant. Electron. **QE-2** (1966), 707.

[39] KUDRIAVTSEVA A., SOKOLOVSKAIA A., GAZENGEL J, PHU XUAN N., RIVOIRE G., Opt. Commun. **26** (1978), 446.

[40] *Obrashchenie volnovego fronta opticheskogo izlucheniya v nelineynykh sredakh*, Ed. Institut prikladnoy fiziki AN SSSR, Gorkiy 1979.

[41] Von Der Linde D., Maier M., Kaiser W., Phys. Rev. 178 (1969), 11.

[42] Carman R. L., Shimizu F., Wang C. S., Bloembergen N., Phys. Rev. A. 2 (1970), 60.

[43] Akhmanov S. A., Drabovich K. N., Sukhorukov A. P., Chirkin A. S., JETP 32 (1971), 266 (transl. from ZhETF 59 (1970), 485).

[44] Wang C. S., Phys. Rev. 182 (1969), 182.

[45] Carman R. L., Mack M. E., Shimizu F., Bloembergen N., Phys. Rev. Lett. 23 (1969), 1327.

[46] Saikan S., Opt. Commun., 6 (1972), 77.

[47] Chatelet M., Oksengorn B., Chem. Phys. Lett. 36 (1975), 73.

[48] Ferrier J. L., Phu xuan N., Rivoire G., Measures–Regulation–Automatisme 45 (1980), 53.

[49] Gazengel J., Ferrier J. L., Phu Xuan N., Rivoire G., Abstracts of the IX Conf. on Quantum Electron. and Nonlinear Optics, Poznań, Poland, April 23–26, 1980, Section B, 29.

[50] Gazengel J., Phu Xuan N., Rivoire G., Opt. Acta 26 (1979), 1245.

[51] Kneipp H., Planner A., Abstracts of the V Polish Conference on Radiospectroscopy and Quant. Electron., Poznań, April. 24–27, 1972, 235.

[52] Gazengel J., Rivoire G., Opt. Acta 26 (1979), 483.

[53] Ferrier J. L., Planner A., Rivoire G., Accepted to pub. in Acta Phys. Polonica, 1981.

[54] Gazengel J., Ph. D. dissertation, Angers, France, 1980.

[55] Shen Y. R., Self focusing: Experimental, [in] Progress in Quant. Electron. Vol. 4, J. H. Sanders, S. Stenholm Eds., Pergamon Press, Oxford 1976, 1.

[56] Marburger J. H., Self focusing: Theory, [in] Progress in Quant. Electron. Vol. 4, J. H. Sanders, S. Stenholm Eds., Pergamon Press, Oxford 1976, 35.

Рубиновый лазер с пассивным синхронизированием модов: типичная конструкция и использование её для исследований вынужденного рамановского рассеяния

В работе описаны результаты многолетних исследований, произведённых авторами, по строению и действию рубинового лазера с пассивным синхронизированием модов, а также использование его для исследований нестационарности в явлении вынужденного рамановского рассеяния (SRS) в жидкостях.

В части, касающейся лазера, содержится: краткий исторический очерк, спектральный и временной анализ формы резонансной линии оптического резонатора лазера, условия получения синхронизации модов с помощью насыщаемого абсорбента, конструкция лазерной головки, конструкция оптического резонатора, система питания лампы-вспышки и генерирование её вспышек, селектор пикосекундных импульсов. В части, касающейся SRS, содержатся: характеристика явления SRS с учётом нестационарного процесса, результаты измерений пороговых интенсивностей возбуждающего пучка SRS. На основе этих результатов обсуждено влияние релаксации молекулярных колебаний на усиление рамановского пучка в жидкостях, а также сделаны выводы относительно природы и взаимодействия явления самофокусировки света.

В конечной части работы обсуждены результаты наблюдения явления самосинхронизации модов в рубиновом лазере со свободной эмиссией, а также результаты измерений зависимости числа возбуждённых пикосекундных импульсов (появляющихся в течение одной вспышки лазера) от толщины слоя насыщаемого абсорбента.